AIP | The Journal of Chemical Physics

Understanding cross-polarization (CP) NMR experiments through dipolar truncation

Manoj Kumar Pandey, Zeba Qadri, and Ramesh Ramachandran

Citation: J. Chem. Phys. **138**, 114108 (2013); doi: 10.1063/1.4794856
View online: http://dx.doi.org/10.1063/1.4794856
View Table of Contents: http://jcp.aip.org/resource/1/JCPSA6/v138/i11
Published by the American Institute of Physics.

Understanding cross-polarization (CP) NMR experiments through dipolar truncation

Manoj Kumar Pandey, Zeba Qadri, and Ramesh Ramachandran[a)]
Department of Chemical Sciences, Indian Institute of Science Education and Research (IISER) Mohali, Sector 81, Manauli P.O. Box-140306, Mohali, Punjab, India

(Received 5 December 2012; accepted 25 February 2013; published online 19 March 2013)

A theoretical model based on the phenomenon of dipolar truncation is proposed to explain the nuances of polarization transfer from abundant to less-abundant nuclei in cross-polarization (CP) NMR experiments. Specifically, the transfer of polarization from protons to carbons (in solids) in strongly coupled systems is described in terms of effective Hamiltonians based on dipolar truncation. Through suitable model spin systems, the important role of dipolar truncation in the propagation of spin polarization in CP experiments is outlined. We believe that the analytic theory presented herein provides a convenient framework for modeling polarization transfer in strongly coupled systems. © *2013 American Institute of Physics*. [http://dx.doi.org/10.1063/1.4794856]

I. INTRODUCTION

Understanding the mechanism of polarization transfer among nuclear spins remains an exciting area of research,[1–3] primarily due to its utility in design/interpretation of NMR experiments/experimental data. Although, NMR measurements are made in bulk, the underlying theory routinely employed to describe/interpret experiments often comprises of finite number of spins. In an alternate approach, an analytic model is presented to explain the mechanism of polarization transfer among spins in a strongly coupled network. To demonstrate this aspect, the cross-polarization (CP) experiment due to Hartmann-Hahn[4] is employed as a test case in our studies. In combination with magic angle spinning (MAS),[5] the CP-MAS experiment[6,7] forms a vital building block in the design of multi-dimensional solid-state NMR experiments for studying less sensitive/abundant nuclei. With the availability of higher magnetic field strengths and faster spinning frequencies, sophisticated variants to the original CP methodology[8–11] have emerged in recent past. However, along with the progress on the experimental front, a development of analytic theory is essential for designing sophisticated experiments and quantifying experimental results. In particular, understanding the mechanism of polarization transfer among nuclear spins in a coupled spin network is essential for developing mathematical models for quantifying experimental data.

In general, the analytic description of polarization transfer in strongly coupled systems is hindered owing to the co-existence of stronger and weaker couplings in the system. Often, polarization transfer to weakly coupled spins is diminished by the influence of other stronger couplings in the system, a phenomenon commonly referred to as dipolar truncation[12] in NMR. Consequently, analytic treatments based on isolated spin-pair models yield ambiguous results and are of limited utility in the weak-coupling regime. To this end, alternate descriptions in the form of thermodynamic models[13] based on the concept of spin temperature[3,14] have also been invoked in the past to explain the experimental observations in CP experiments.

As an alternative to existing methods, an analytic model built on the concept of "dipolar truncation" is proposed to explain the propagation of spin polarization in CP experiments. The complexities arising from the spin dimension are carefully evaded through the derivation of effective Hamiltonians based on dipolar truncation. Employing the "truncated effective Hamiltonians," the mechanism of polarization transfer in a wide range of model systems is investigated. The validity of the proposed analytic approach is verified through a rigorous comparison with simulations based on exact numerical methods. In Sec. II, a detailed description of polarization transfer in CP-MAS experiments through truncated effective Hamiltonians is described. Based on the analytic simulations, the results emerging from the current study are summarized in Sec. III.

II. RESULTS AND DISCUSSION

In the standard CP experiment of Hartmann and Hahn, polarization transfer between spins (I and S) is induced when the amplitudes of the RF fields ($\upsilon_{RF,S}$, $\upsilon_{RF,I}$) employed are adjusted to the matching condition, $\upsilon_{RF,S} = \upsilon_{RF,I}$. By contrast, the CP matching conditions in MAS experiments have a profound dependence on the spinning frequency (υ_r) of the sample. Depending on the spinning frequency and the RF amplitudes employed, CP-MAS experiments in the solid-state are primarily classified into (1) first-order and (2) second-order schemes. To facilitate polarization transfer under MAS, the amplitude of the RF fields in first-order CP schemes is adjusted to one of the matching conditions[7] given by $|\upsilon_{RF,S} \pm \upsilon_{RF,I}| = \upsilon_r$ or $2\upsilon_r$. However, the matching conditions in second-order schemes[9–11,15] remain identical to the original CP experiment ($\upsilon_{RF,S} = \upsilon_{RF,I}$). The details of such schemes

a)Author to whom correspondence should be addressed. Electronic mail: rramesh@iisermohali.ac.in.

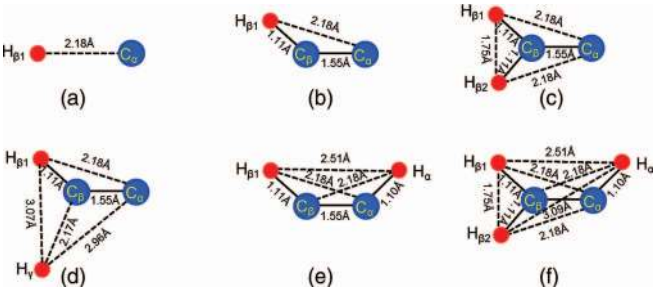

FIG. 1. Model systems employed for describing the polarization transfer in CP experiments.

are well documented and will not be elaborated upon in this article.

Here in this article, we confine our discussion towards identifying the factors responsible for the propagation of spin polarization from $^1H \rightarrow {}^{13}C$ in CP experiments. To realize this goal, a pedagogical description comprising of two ($C_\alpha H_\beta$), three ($C_\alpha C_\beta H_{\beta 1}$), four ($C_\alpha C_\beta H_{\beta 1} H_{\beta 2}$; $C_\alpha C_\beta H_{\beta 1} H_\gamma$; $C_\alpha H_\alpha C_\beta H_\beta$), and five ($C_\alpha H_\alpha C_\beta H_{\beta 1} H_{\beta 2}$) spin model systems is employed (see Figure 1) in our studies. Since the ^{13}C–^1H, ^1H–^1H dipolar coupling constants in the chosen model systems are prototypes of the coupling constants prevalent in typical amino acid residues/peptides, we believe that the current study would improve the accuracy of the structural constraints derived using solid-state NMR.

To begin with, numerical simulations (based on SPINEVOLUTION[16]) depicting polarization transfer from $^1H \rightarrow {}^{13}C_\alpha$ in first-order CP experiments are presented in Figure 2. Since, bio-molecular applications of solid-state NMR entail faster spinning frequencies (for better resolution), the amplitudes of the RF fields in the simulations were adjusted to $|\upsilon_{RF,S} - \upsilon_{RF,I}| = \upsilon_r$, i.e. ($\upsilon_r = 60$ kHz, $\upsilon_{RF,I} = 20$ kHz, $\upsilon_{RF,S} = 40$ kHz) and phase shifted by 180°. To explain the nuances of polarization transfer in first-order based

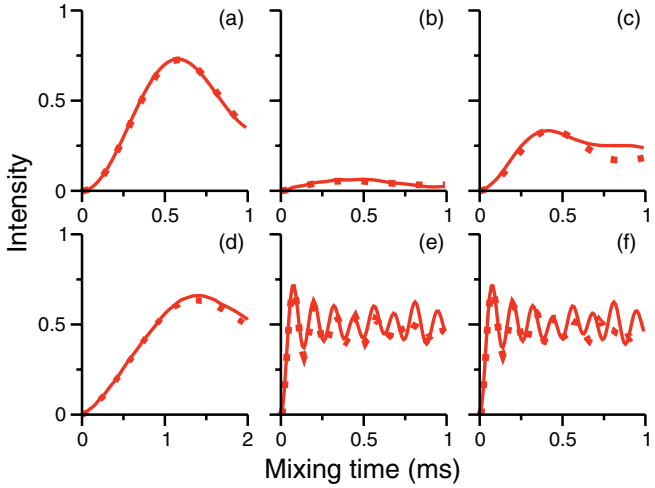

FIG. 2. CP Simulations depicting the polarization transfer to C_α in the model systems presented in Figure 1. The RF amplitudes correspond to $\upsilon_{RF,S} = 40$ kHz, $\upsilon_{RF,I} = 20$ kHz and the phases shifted by 180°. All the simulations were performed at $\upsilon_r = 60$ kHz. The solid lines correspond to analytic simulations, while dots represent numerical simulations based on SPINEVOLUTION.[16]

CP experiments, we begin our discussion with the profiles depicted in panels (b) and (c) (Figure 2). As depicted, polarization transfer to $^{13}C_\alpha$ in the three-spin system $C_\alpha C_\beta H_{\beta 1}$ (see panel (b)) is diminished significantly in contrast to the isolated spin pair system (panel (a)). This decrease in the CP efficiency is often attributed to the presence of the stronger C_β–$H_{\beta 1}$ dipolar coupling and is commonly referred to as dipolar truncation[12] in solid-state NMR. Interestingly, inclusion of an additional proton to the beta carbon (C_β) (four spin model, Figure 1(c)) improves the overall transfer efficiency to C_α (see Figure 2(c)).

This result seems counter-intuitive, in view of the fact that the three-spin model $C_\alpha C_\beta H_{\beta 1}$ (Figure 1(b)) comprises of fewer stronger couplings (C_β-$H_{\beta 1}$) in comparison to the four-spin model $C_\alpha C_\beta H_{\beta 1} H_{\beta 2}$ (stronger couplings in the form of C_β–$H_{\beta 1}$ and C_β–$H_{\beta 2}$). Hence, an analytic theory is essential for understanding the mode of polarization transfer from multiple spin sites (say ^1H) to the desired target spin (say ^{13}C) in strongly coupled systems. In Secs. II A–II C, a brief introduction to the theoretical methods employed for studying CP-MAS experiments is illustrated.

A. Theory

1. Spin Hamiltonian under MAS

To elucidate the mechanism of polarization transfer in CP-MAS experiments, a model system ($I_N S_M$) comprising of N-carbons (I = ^{13}C) and M-protons (S = ^1H) is employed in our studies. Under sample rotation, the nuclear spin Hamiltonian is time-dependent,[17] and is conveniently expressed in the rotating frame by

$$H(t) = \sum_{\lambda=I,S} H_\lambda(t) + H_{IS}(t) + H_{RF}. \tag{1}$$

The chemical shift and the dipolar interactions associated with the spins (I and S) are represented through H_λ. For example, the Hamiltonian for a system comprising of N-spins is represented by

$$H_I(t) = \sum_{i=1}^{N} \sum_{m=-2}^{2} \omega_{I_i}^{(m)} e^{im\omega_r t} I_{iz} + \sum_{\substack{i,j=1,\\ i\neq j}}^{N} \sum_{\substack{m=-2,\\ m\neq 0}}^{2} \omega_{I_i I_j}^{(m)} e^{im\omega_r t} \times \left[2I_{iz}I_{jz} - \tfrac{1}{2}(I_i^+ I_j^- + I_i^- I_j^+)\right]. \tag{2}$$

Due to the restricted mobility, the spin interactions in the solid-state are anisotropic and are expressed in terms of second rank tensors. The spatial anisotropy associated with the chemical shift and dipolar interactions are depicted through "m" ($m = -2$ to 2) and are represented by $\omega_\lambda^{(m)}$, $\omega_{\lambda_1\lambda_2}^{(m)}$, respectively. For the sake of convenience, the isotropic part of the chemical shift interaction (represented by $\omega_\lambda^{(0)}$) is included along with the anisotropic interaction in our description. The interaction Hamiltonian H_{IS} depicts the coupling between the spins and is represented by

$$H_{IS}(t) = \sum_{i=1}^{N} \sum_{j=1}^{M} \sum_{\substack{m=-2,\\ m\neq 0}}^{2} \omega_{I_i S_j}^{(m)} e^{im\omega_r t} 2I_{iz}S_{jz}. \tag{3}$$

In the rotating frame, the oscillating radio-frequency (RF) field is time-independent and is represented by

$$H_{RF} = \omega_{RF,I} \sum_{i=1}^{N} I_{ix} + \omega_{RF,S} \sum_{j=1}^{M} S_{jx}. \tag{4}$$

To simplify the description of the spin dynamics, the Hamiltonian in the rotating frame (Eq. (1)) is transformed using a set of unitary transformations defined below,

$$\tilde{H}(t) = U_2 U_1 \, H(t) \, U_1^{-1} U_2^{-1}. \tag{5}$$

The initial transformation operator $U_1 = \exp(i\frac{\pi}{2}\sum_{i=1}^{N} I_{iy})$ $\exp(i\frac{\pi}{2}\sum_{j=1}^{M} S_{jy})$ transforms the Hamiltonian into a tilted rotating frame, wherein the RF part of the Hamiltonian is quantized along the z-axis. To deduce the optimum CP conditions, the Hamiltonian in the tilted rotating frame is further transformed into the RF interaction frame through the transformation operator $U_2 = \exp(i\omega_{RF,I} t \sum_{i=1}^{N} I_{iz})$ $\exp(i\omega_{RF,S} t \sum_{j=1}^{M} S_{jz})$.

To facilitate analytic description, the Hamiltonian in the RF interaction frame is further split into single-spin and two-spin interactions and is re-expressed in terms of spherical tensor operators. The single-spin Hamiltonian depicts both the isotropic and anisotropic chemical shift interactions and is expressed in terms of single-quantum (SQ) operators,

$$\tilde{H}_{Single}(t) = -\frac{1}{\sqrt{2}}.(\sqrt{2})^{N+M-2} \sum_{m=-2}^{2} \sum_{i=1}^{N} \omega_{I_i}^{(m)} \begin{bmatrix} iT^{(1)1}(I_i) \exp\left(i\,[m\omega_r + \omega_{RF}]\,t\right) - \\ iT^{(1)-1}(I_i) \exp\left(i\,[m\omega_r - \omega_{RF}]\,t\right) \end{bmatrix}. \tag{6}$$

In a similar vein, the two-spin interactions comprising of homonuclear and heteronuclear dipolar interactions are expressed in terms of zero-quantum (ZQ) and double-quantum (DQ) operators,

$$\tilde{H}_{Hetero}^{(DQ)}(t) = -\frac{1}{2}(\sqrt{2})^{N+M-2} \sum_{i=1}^{N} \sum_{j=1}^{M} \sum_{\substack{m=-2, \\ m\neq 0}}^{2} \omega_{I_i S_j}^{(m)} \begin{bmatrix} T^{(2)2}(I_i S_j) \exp\left(i\left[m\omega_r + \left(\omega_{RF,I} + \omega_{RF,S}\right)\right]t\right) + \\ T^{(2)-2}(I_i S_j) \exp\left(i\left[m\omega_r - \left(\omega_{RF,I} + \omega_{RF,S}\right)\right]\right) \end{bmatrix}, \tag{7a}$$

$$\tilde{H}_{Hetero}^{(ZQ)}(t) = (\sqrt{2})^{N+M-2} \sum_{i=1}^{N} \sum_{j=1}^{M} \sum_{\substack{m=-2, \\ m\neq 0}}^{2} \frac{1}{2}\omega_{I_i S_j}^{(m)} \begin{bmatrix} \left[\frac{1}{\sqrt{3}}T^{(0)0}(I_i S_j) + \frac{1}{\sqrt{2}}T^{(1)0}(I_i S_j) + \frac{1}{\sqrt{6}}T^{(2)0}(I_i S_j)\right] * \\ \exp\left(i\left[m\omega_r + \left(\omega_{RF,I} - \omega_{RF,S}\right)\right]t\right) \\ + \\ \left[\frac{1}{\sqrt{3}}T^{(0)0}(I_i S_j) - \frac{1}{\sqrt{2}}T^{(1)0}(I_i S_j) + \frac{1}{\sqrt{6}}T^{(2)0}(I_i S_j)\right] * \\ \exp(i[m\omega_r - (\omega_{RF,I} - \omega_{RF,S})]t) \end{bmatrix}, \tag{7b}$$

$$\tilde{H}_{Homo}^{DQ}(t) = -\frac{3}{4}.(\sqrt{2})^{N+M-2} \sum_{\substack{i,j=1 \\ i<j}}^{N} \sum_{\substack{m=-2, \\ m\neq 0}}^{2} \omega_{I_i I_j}^{(m)} \begin{bmatrix} T^{(2)2}(I_i I_j) \exp\left(i\left[m\omega_r + 2.\omega_{RF,I}\right]t\right) + \\ T^{(2)-2}(I_i I_j) \exp\left(i\left[m\omega_r - 2.\omega_{RF,I}\right]t\right) \end{bmatrix}, \tag{8a}$$

$$\tilde{H}_{Homo}^{ZQ}(t) = \sqrt{\frac{3}{8}}.(\sqrt{2})^{N+M-2} \sum_{\substack{i,j=1 \\ i<j}}^{N} \sum_{\substack{m=-2, \\ m\neq 0}}^{2} \omega_{I_i I_j}^{(m)} T^{(2)0}(I_i I_j) \exp\left(im\omega_r t\right). \tag{8b}$$

Since the Hamiltonian under MAS is time-dependent and periodic, analytic descriptions of MAS NMR experiments are often based on the framework provided by either average Hamiltonian theory[1,18] or Floquet theory.[19] Here in this article, the multipole-multimode (MMFT[20]) formulation of Floquet theory[19] is employed for describing CP experiments. Although, effective Floquet Hamiltonians[21] based on this approach have been derived and are well documented in the literature,[20,22–26] the important stages in the calculations are summarized below for the sake of continuity.

2. MMFT

In the MMFT approach, the time-dependent Hamiltonian (see Eqs. (6)–(8)) is transformed into a time-independent Hamiltonian (commonly referred to as Floquet Hamiltonian) via Fourier series expansion. Consequently, the nuclear spin states ($|IM\rangle$) are dressed with the Fourier indices associated with the various modulations in the system, i.e., $|IM, m, m_1, m_2\rangle$. The periodic modulation imposed by sample rotation is depicted through the Fourier index "m," while the indices m_1, m_2 depict the modulations due to the oscillating

RF fields on spins I and S, respectively. To reduce the complexity in the infinite dimensional Floquet vector space, effective Floquet Hamiltonians based on the method of contact transformation[27] are derived. To facilitate the implementation of the contact transformation procedure, the Floquet Hamiltonian is re-expressed as a sum comprising of a zero-order (H_0) and a perturbing Hamiltonian (H_1),

$$H_F = H_0 + H_1. \tag{9}$$

In general, the zero-order Hamiltonian in the Floquet-Hilbert space[28] is expressed through operators that are diagonal both in the spin and Fourier space (i.e., $\langle IM, m, m_1, m_2|I_F^{(m)}|IM, m', m_1', m_2'\rangle = m\,\delta_{m',m}\delta_{m_1',m_1}\delta_{m_2',m_2}$),

$$H_0 = \omega_r I_F^{(m)} + \omega_{RF,I} I_{F_1}^{(m_1)} + \omega_{RF,S} I_{F_2}^{(m_2)}. \tag{10}$$

The perturbing Floquet Hamiltonian H_1 is defined in terms of Floquet operators that are off diagonal in the Fourier space,

$$H_1 = H_F^{(I)} + H_F^{(S)} + H_F^{(IS)}, \tag{11}$$

$$H_F^{(I)} = \sum_{m,m_1}\sum_{i=1}^{N}\sum_{q=-1}^{1} G_{m,m_1}^{(1)q}(I_i)\, iT_{m,m_1}^{(1)q}(I_i) + \sum_{\substack{i,j=1,\\ i<j}}^{N}\sum_{m,m_1}\sum_{k=0}^{2}\sum_{q=-k}^{k}\left[G_{m,m_1}^{(k)q}(I_iI_j)T_{m,m_1}^{(k)q}(I_iI_j)\right], \tag{12a}$$

$$H_F^{(S)} = \sum_{m,m_2}\sum_{i=1}^{M}\sum_{q=-1}^{1} G_{m,m_1}^{(1)q}(S_i)\, iT_{m,m_2}^{(1)q}(S_i) + \sum_{\substack{i,j=1,\\ i<j}}^{M}\sum_{m,m_2}\sum_{k=0}^{2}\sum_{q=-k}^{k}\left[G_{m,m_2}^{(k)q}(S_iS_j)T_{m,m_2}^{(k)q}(S_iS_j)\right], \tag{12b}$$

$$H_F^{(IS)} = \sum_{m,m_1,m_2}\sum_{i=1}^{N}\sum_{j=1}^{M}\sum_{k=0}^{2}\sum_{q=-k}^{k} \times \left[G_{m,m_1,m_2}^{(k)q}(I_iS_j)T_{m,m_1,m_2}^{(k)q}(I_iS_j)\right]. \tag{12c}$$

The "G" coefficients in Eq. (12) could be deduced from the coefficients described in Eqs. (6)–(8) inclusive of the numerical constants (i.e., $G_{m,m_1}^{(1)\pm1}(I_i) = \mp\frac{1}{\sqrt{2}}.(\sqrt{2})^{N+M-2}\omega_{I_i}^{(m)}$, $G_{m,m_1}^{(k)q}(I_iI_j) = -\frac{3}{4}.(\sqrt{2})^{N+M-2}\omega_{I_iI_j}^{(m)}$, etc.) and are similar to our earlier description.[26]

The second stage in the calculation involves the folding of the off-diagonal contributions due to H_1. In contrast to the standard perturbation theory, the perturbation corrections in the contact transformation method are derived through unitary transformations and are expressed in terms of operators. The transformed Hamiltonian (referred to as effective Hamiltonian) to second-order after a single transformation is represented by

$$\begin{aligned} H_F^{eff} &= \exp(iS_1)H_F\exp(-iS_1) \\ &= H_0^{(1)} + H_1^{(1)} + H_2^{(1)}, \end{aligned}$$

$$\begin{aligned} H_0^{(1)} &= H_0, \\ H_1^{(1)} &= H_1 + i[S_1, H_0], \\ H_2^{(1)} &= \frac{i}{2}[S_1, H_1]. \end{aligned} \tag{13}$$

In the above equation, the transformation function S_1 is expressed in terms of operators whose coefficients are carefully chosen to compensate the off-diagonality due to H_1, i.e., $-H_1 = i[S_1, H_0]$. The term $H_n^{(1)}$ in Eq. (13) denotes the nth - order correction to the zero-order Hamiltonian resulting from a single transformation.

The final stage involves the description of the time-evolution of the system through the quantum-Liouville equation given below,

$$i\hbar\frac{d\rho(t)}{dt} = \left[H_F^{eff}, \rho(t)\right]. \tag{14}$$

To facilitate analytic description of polarization transfer in CP experiments, Eq. (14) is reformulated in terms of coupled differential equations,[29,30]

$$i\hbar\frac{d}{dt}\Phi_q^{(k)}(\lambda, t) = \underbrace{Trace[T^{(k)-q}(\lambda)[H, T^{(k')q'}(\lambda')]]}_{P^{(k')q'}(\lambda')}\ \Phi_{q'}^{(k')}(\lambda', t). \tag{15}$$

A brief description of first-order and second-order CP experiments based on the effective Hamiltonian approach is summarized in Sec. II B.

B. Effective Floquet Hamiltonians for first-order and second-order CP experiments

When the amplitudes of the RF fields are adjusted to one of the matching conditions[7] ($|\upsilon_{RF,S} \pm \upsilon_{RF,I}| = \upsilon_r$ or $2\upsilon_r$), a part of the two-spin Hamiltonian (refer to Eq. (7b)) becomes time-independent under MAS conditions (commonly referred to as "recoupled Hamiltonian"). In such cases, the recoupled Hamiltonian is included as a diagonal contribution[22,26] along H_1 and the transformation function is carefully chosen only to compensate the off-diagonal contributions in H_1. The second-order corrections ($H_2^{(1)}$) to the zero-order Hamiltonian are composed of single-spin, two-spin, and three-spin operators. For a given system, the single-spin operators to second-order result from cross-terms between (a) single-spin operators (say CSA × CSA) and (b) two-spin operators associated with the same pair of spin, while the cross-terms between single-spin and two-spin operators in (CSA × dipolar interactions) result in two-spin operators. The cross-terms between different pairs of dipolar interactions (with at least one-spin being common) result in three-spin operators. A detailed description of the second-order contributions is summarized in Table I (refer to the Appendix), along with a generalization for extensions to N-coupled spin ($I = 1/2$) systems.

Employing the results summarized in Table I, the first-order contribution to the effective Hamiltonian in CP

experiments is expressed in terms of two-spin operators,

$$H_1^{(1)} = H_{1,dia} = \underbrace{\sum_{i=1}^{N}\sum_{j=1}^{M}\sum_{k=0}^{2} A^{(k)0}(I_i S_j) T^{(k)0}(I_i S_j)}_{\text{Two-Spin}}. \tag{16}$$

In a similar vein, the second-order contributions are composed of single spin and three-spin operators as represented below,

$$H_2^{(1)} = \underbrace{\sum_{\lambda=I,S}\sum_{i} B^{(1)0}(\lambda_i).iT^{(1)0}(\lambda_i)}_{\text{Single-spin}} + \underbrace{\sum_{i}^{N}\sum_{\substack{r,j=1\\ j<r}}^{M} B_1^{(k)0}(I_i S_j S_r) T^{(k)0}(I_i S_j S_r) + \sum_{\substack{i,j=1\\ i<j}}^{N}\sum_{r=1}^{M} B_1^{(k)0}(I_i I_j S_r) T^{(k)0}(I_i I_j S_r)}_{\text{Three-Spin}}. \tag{17}$$

Based on Eq. (13), the effective Hamiltonian describing first-order CP experiments is represented by

$$H_F^{eff} = H_0^{(1)} + H_1^{(1)} + H_2^{(1)}. \tag{18}$$

Subsequently, employing the effective Hamiltonians in Eq. (15), the polarization transfer between an isolated spin pair (IS) (panel (a), Figure 2) is described using a set of coupled differential equations[22,23,26] comprising of single-spin ($\Phi_0^{(1)}(\lambda, t), \lambda = I, S$) and two-spin polarizations ($\Phi_0^{(k)}(IS, t), k = 0, 1, 2$),

$$\begin{aligned}
i\hbar\frac{d}{dt}\Phi_0^{(1)}(I,t) &= \sum_{k=0}^{2} P^{(k)0}(IS)\,\Phi_0^{(k)}(IS,t),\\
i\hbar\frac{d}{dt}\Phi_0^{(1)}(S,t) &= \sum_{k=0}^{2} P^{(k)0}(IS)\,\Phi_0^{(k)}(IS,t),\\
i\hbar\frac{d}{dt}\Phi_0^{(k)}(IS,t) &= \sum_{\lambda=I,S} P^{(1)0}(\lambda)\,\Phi_0^{(1)}(IS,t)\\
&\quad + \sum_{\lambda=I,S}\sum_{k=0}^{2} P^{(k)0}(IS)\,\Phi_0^{(k)}(\lambda,t).
\end{aligned} \tag{19}$$

When the magnitude of the coefficients associated with the single-spin operators exceeds the magnitude of the coefficients associated with two-spin operators (i.e., $P^{(1)0}(\lambda) > P^{(k)0}(IS)$), the above coupled-differential equations reduce to a much simpler form given below,

$$\begin{aligned}
i\hbar\frac{d}{dt}\Phi_0^{(1)}(I,t) &= 0,\\
i\hbar\frac{d}{dt}\Phi_0^{(1)}(S,t) &= 0,\\
i\hbar\frac{d}{dt}\Phi_0^{(k)}(IS,t) &= \sum_{\lambda=I,S} P^{(1)0}(\lambda)\,\Phi_0^{(1)}(IS,t).
\end{aligned} \tag{20}$$

Consequently, the single-spin polarizations $\Phi_0^{(1)}(\lambda, t)$ remain invariant and polarization transfer among spins is unobserved in CP experiments.

While the above differential equations provide an intuitive framework for understanding the spin dynamics in an isolated spin pair, their utility in providing analytic insights is limited primarily due to the increase in the number of differential equations in strongly coupled systems. For example, the effective Hamiltonian of a three-spin system in the Liouville space comprises of three single-spin, nine two-spin (three for a pair), and seven three-spin operators. Hence, descriptions based on the effective Hamiltonian approach are less suited for studying polarization transfer among strongly coupled spin systems. To alleviate this problem, an alternate approach in the form of "truncated effective Hamiltonians" employing fewer differential equations is proposed in Sec. II C.

C. Concept of truncated effective Hamiltonians

To describe the mechanism of polarization transfer in strongly coupled systems, the effective Hamiltonians derived in Sec. II B are restructured based on the phenomenon of dipolar truncation. Employing this approach, truncated effective Hamiltonians are proposed by retaining only the dominant contributions in the effective Hamiltonians. Although, such an approach reduces the number of coupled differential equations in the Liouville space, the validity of such approximations could only be verified through a comparison between analytic simulations emerging from the truncated Hamiltonians and the exact numerical simulations comprising of the entire spin system of interest. Employing the model systems depicted in Figure 1, truncated effective Hamiltonians are proposed for describing the polarization transfer observed in first-order and second-order CP experiments.

1. First-order CP experiments

As illustrated through the simulations depicted in Figure 2(b), the stronger dipolar interaction due to C_β–$H_{\beta 1}$ ($\omega_{C_\beta H_{\beta 1}}$) truncates the polarization transfer to C_α (i.e., $\omega_{C_\beta H_{\beta 1}} > \omega_{C_\alpha H_{\beta 1}}$) in the three-spin system $C_\alpha C_\beta H_{\beta 1}$. Consequently, a truncated effective Hamiltonian in the form of $H_{F,Three}^{(eff)T}$ comprising of $T^{(k)0}(C_\beta H_{\beta_1})$ and single-spin

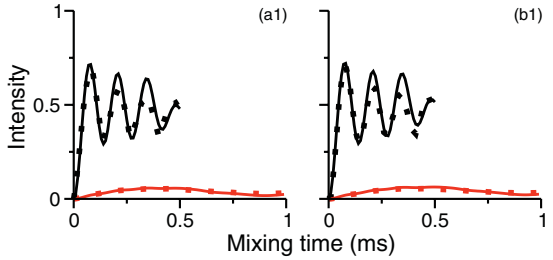

FIG. 3. Simulations depicting the polarization transfer to C_α (red) and C_β (black) in the model three-spin system (Figure 1(b)). The analytic simulations in panel (a1) correspond to the complete effective Hamiltonian, while those depicted in panel (b1) correspond to the reduced Hamiltonian. Solid lines depict analytic simulations, while the numerical simulations are indicated by dots.

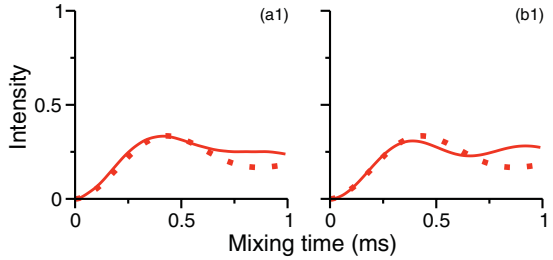

FIG. 4. Simulations depicting polarization transfer to C_α in $C_\alpha C_\beta H_{\beta 1} H_{\beta 2}$ (Figure 1(c)). The analytic simulations comprise of both the complete (a1) and truncated (b1) effective Hamiltonians (comprising of only $C_\alpha H_{\beta 2}$). The analytic simulations presented are compared with the exact numerical simulations (dots) involving all the four spins in $C_\alpha C_\beta H_{\beta 1} H_{\beta 2}$.

operators $T^{(1)0}(C_\beta)$, $T^{(1)0}(H_{\beta_1})$ is proposed for describing the polarization transfer observed in $C_\alpha C_\beta H_{\beta 1}$ (Figure 1(b)). Due to the smaller magnitude of the second-order coefficients (see Table I), the contributions from the three-spin operators are neglected and the truncated effective Hamiltonian is expressed only in terms of single-spin and two-spin operators:

$$H^{(eff)T}_{F,Three,C_\beta} = \sum_{k=0}^{2} A^{(k)0}(C_\beta H_{\beta_1}) T^{(k)0}(C_\beta H_{\beta_1}) + \sum_{\lambda = C_\beta, H_{\beta_1}} B^{(1)0}(\lambda).iT^{(1)0}(\lambda). \quad (21)$$

To test the validity of this approach, analytic simulations depicting polarization transfer to C_α and C_β in $C_\alpha C_\beta H_{\beta 1}$ are compared in Figure 3 with exact numerical simulations (inclusive of all three-spins). For illustrative purposes, the analytic simulations emerging from both effective (panel (a1)) and truncated (panel (b1)) Hamiltonians are compared with exact numerical simulations. In contrast to the effective Hamiltonian approach, polarization transfer to C_β (depicted in panel (b1)) is simulated within a reduced subspace comprising of spins C_β and $H_{\beta 1}$. Hence, the truncated effective Hamiltonian approach provides an alternate framework for describing the dipolar truncation effect observed in $C_\alpha C_\beta H_{\beta 1}$.

To explain the enhanced polarization transfer observed in $C_\alpha C_\beta H_{\beta 1} H_{\beta 2}$ (see Figure 2(c)), we propose a model, wherein, polarization transfer to C_β results from only one of the protons, say $H_{\beta 1}$ in $C_\alpha C_\beta H_{\beta 1} H_{\beta 2}$. Consequently, the polarization from $H_{\beta 2}$ is readily transferred to C_α without the destructive influence of the stronger C_β–$H_{\beta 2}$ dipolar coupling. Based on this model, the truncated effective Hamiltonians describing polarization transfer to C_β and C_α are derived and represented by

$$H^{(eff)T}_{F,Four,C_\beta} = \sum_{k=0}^{2} A^{(k)0}(C_\beta H_{\beta_1}) T^{(k)0}(C_\beta H_{\beta_1}) + \sum_{\lambda = C_\beta, H_{\beta_1}} B^{(1)0}(\lambda).iT^{(1)0}(\lambda), \quad (22)$$

$$H^{(eff)T}_{F,Four,C_\alpha} = \sum_{k=0}^{2} A^{(k)0}(C_\alpha H_{\beta_2}) T^{(k)0}(C_\alpha H_{\beta_2}) + \sum_{\lambda = C_\alpha, H_{\beta_2}} B^{(1)0}(\lambda).iT^{(1)0}(\lambda). \quad (23)$$

In a similar vein, the stronger coupling in the form of C_β–$H_{\beta 1}(\omega_{C_\beta H_{\beta 1}})$ truncates the C_β–H_γ dipolar coupling in $C_\alpha C_\beta H_{\beta 1} H_\gamma$ (Figure 2(d)) and facilitates the propagation of spin polarization to C_α. Hence, based on the truncated effective Hamiltonian approach, polarization transfer to C_β and C_α in the model four-spin system $C_\alpha C_\beta H_{\beta 1} H_\gamma$ should result primarily from $H_{\beta 1}$ ($H_{\beta 1} \rightarrow C_\beta$ through $T^{(k)0}(C_\beta H_{\beta_1})$) and H_γ ($H_\gamma \rightarrow C_\alpha$ through $T^{(k)0}(C_\alpha H_\gamma)$), respectively.

To verify the validity of the proposed models based on truncated effective Hamiltonians, analytic simulations emerging from both effective and truncated Hamiltonians were compared with exact numerical simulations. In Figure 4, polarization transfer to C_α in $C_\alpha C_\beta H_{\beta 1} H_{\beta 2}$ is calculated both from the effective (panel (a1)) and truncated effective Hamiltonians (panel (b1)) and compared with exact numerical methods (indicated by dots). As depicted (in Figure 4(b1)), the analytic simulations emerging from the truncated effective Hamiltonians (comprising of C_α and $H_{\beta 2}$) are in good agreement with the four-spin numerical simulations in $C_\alpha C_\beta H_{\beta 1} H_{\beta 2}$. Hence, the truncation effect imposed by the stronger C_β–$H_{\beta 1}$ coupling on C_β–$H_{\beta 2}$ indirectly influences (facilitates) the transfer of polarization from $H_{\beta 2}$ to C_α in $C_\alpha C_\beta H_{\beta 1} H_{\beta 2}$. While the efficiency of transfer from $H_{\beta 2} \rightarrow C_\alpha$ in $C_\alpha C_\beta H_{\beta 1} H_{\beta 2}$ is higher in contrast to the three-spin simulations depicted in Figure 2(b), it is still diminished in comparison to the simulations depicting polarization transfer in an isolated spin pair (see Figure 2(a)). This reduction in efficiency is attributed to the influence of the passive spin $H_{\beta 1}$ through the $H_{\beta 1}$–$H_{\beta 2}$ dipolar coupling in $C_\alpha C_\beta H_{\beta 1} H_{\beta 2}$. Although, matching conditions (say $\omega_{RF,S} = \frac{1}{2}\omega_r$) corresponding to the reintroduction of $H_{\beta 1}$–$H_{\beta 2}$ dipolar interactions are avoided in CP-MAS experiments, their manifestations through second-order cross-terms are inevitable in strongly coupled systems. As summarized in Table I, second-order cross-terms between the ^{1}H–^{1}H dipolar interactions ($H_{H_{\beta 1}-H_{\beta 2}} \times H_{H_{\beta 1}-H_{\beta 2}}$) result in longitudinal single-spin operators $T^{(1)0}(H_{\beta_1})$ and have been incorporated in the truncated effective Hamiltonians (Eqs. (17) and (18)) for better agreements with exact numerical simulations. Hence, the truncated effective Hamiltonian approach provides an adequate framework for the inclusion of both passive and active spins in a reduced subspace within the Liouville space.

In general, depending on the magnitude of the ^{1}H–^{13}C dipolar-coupling constants, the influence of passive spins in

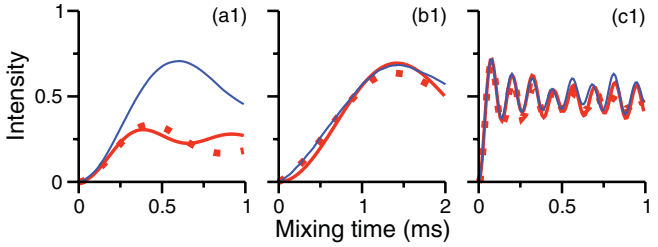

FIG. 5. Simulations highlighting the role of ^{1}H–^{1}H-homonuclear dipolar interactions on polarization transfer to C_α in (a1) $C_\alpha C_\beta$ $H_{\beta 1}H_{\beta 2}$, (b1) $C_\alpha H_\gamma C_\beta H_{\beta 1}$, and (c1) $C_\alpha H_\alpha C_\beta H_{\beta 1}$. The analytic simulations based on the reduced effective Hamiltonian (solid lines in red) are compared with the exact numerical simulations (dots) involving all the four spins in the chosen model systems. The analytic simulations depicted in blue represent the absence of ^{1}H–^{1}H dipolar coupling in the reduced Hamiltonian.

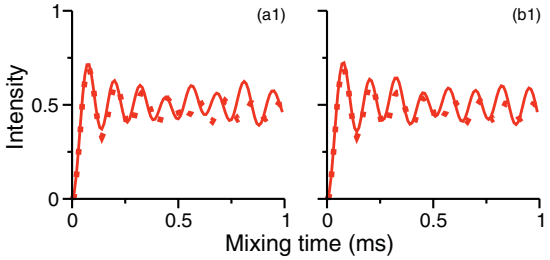

FIG. 6. Simulations depicting polarization transfer to C_α in the model five-spin system depicted ($C_\alpha H_\alpha C_\beta H_{\beta 1}H_{\beta 2}$) in Figure 1(f). The analytic simulations (solid lines) comprising of both the complete (a1) and reduced (b1) effective Hami1tonians are compared with five-spin numerical simulations.

CP experiments varies. To illustrate this aspect, polarization transfer to C_α in $C_\alpha C_\beta H_{\beta 1}H_{\beta 2}$ (Figure 5a1), $C_\alpha C_\beta H_{\beta 1}H_\gamma$ (Figure 5b1), and $C_\alpha H_\alpha C_\beta H_{\beta 1}$ (Figure 5c1) is depicted both in the presence (indicated in red) and absence (indicated in blue) of the second-order cross-terms resulting from the ^{1}H–^{1}H dipolar interactions. As depicted in Figure 5, the analytic simulations from the truncated effective Hamiltonians (indicated in red) are in good agreement with the numerical simulations (dots) in all the model four-spin systems. Due to smaller magnitude of the C_α–$H_{\beta 2}$ dipolar coupling constant, the second-order cross-terms resulting from ^{1}H–^{1}H dipolar interactions have a prominent role in the efficiency of polarization transfer in $C_\alpha C_\beta H_{\beta 1}H_{\beta 2}$ (depicted in blue in panel (a1)). Hence, polarization transfer to C_α in the model four-spin systems (depicted through Figures 1(c)–1(e)) could, in principle, be described within an isolated two-spin framework comprising of C_α–$H_{\beta 2}$, C_α–H_γ, and C_α–H_α dipolar couplings, respectively. The truncated effective Hamiltonians are represented by

$$H^{(eff)T}_{F,Four,C_\alpha} = \sum_{k=0}^{2} A^{(k)0}(C_\alpha H_\alpha)T^{(k)0}(C_\alpha H_\alpha) + \sum_{\lambda=C_\alpha,H_\alpha} B^{(1)0}(\lambda).iT^{(1)0}(\lambda), \quad (24)$$

$$H^{(eff)T}_{F,Four,C_\beta} = \sum_{k=0}^{2} A^{(k)0}(C_\beta H_{\beta_1})T^{(k)0}(C_\beta H_{\beta_1}) + \sum_{\lambda=C_\beta,H_{\beta_1}} B^{(1)0}(\lambda).iT^{(1)0}(\lambda). \quad (25)$$

In a similar vein, polarization transfer to C_α in the model five-spin system $C_\alpha H_\alpha C_\beta H_{\beta 1}H_{\beta 2}$ was simulated using truncated effective Hamiltonians (see Figure 6).

Based on the extensive analytic simulations, a schematic decomposition of polarization transfer in the chosen model systems is summarized through Figure 7. Hence, in a strongly coupled system, dipolar truncation seems to be the driving force behind the propagation of spin polarization in first-order based CP experiments. In Sec. II C 2, we explore the suitability of truncated effective Hamiltonians in understanding the propagation of spin polarization in second-order CP experiments.

2. Second-order CP experiments

To minimize the effects of sample heating (due to RF fields) and facilitate implementation of CP-MAS experiments at faster spinning frequencies, schemes based on second-order recoupling were preferred over first-order CP experiments. In contrast to first-order based schemes, the three-spin operators (see Table I) resulting from cross-terms between different pairs of dipolar interactions such as (a) heteronuclear X heteronuclear dipolar interactions (say C_1–H_1 X C_1–H_2) and (b) cross-terms from homonuclear X heteronuclear interactions (such as C_1-H_1 X H_1–H_2) facilitate the propagation of polarization in second-order based schemes.

For example, in PAIN-CP[11] type experiments, polarization transfer from carbon to nitrogen is mediated through a proton that is coupled to both the spins (i.e., second-order cross-terms resulting from C–H_1 X N–H_1), while in second-order recoupling (SOCP)[10] experiments cross-terms from both (a) and (b) aid in polarization transfer. In Figure 8,

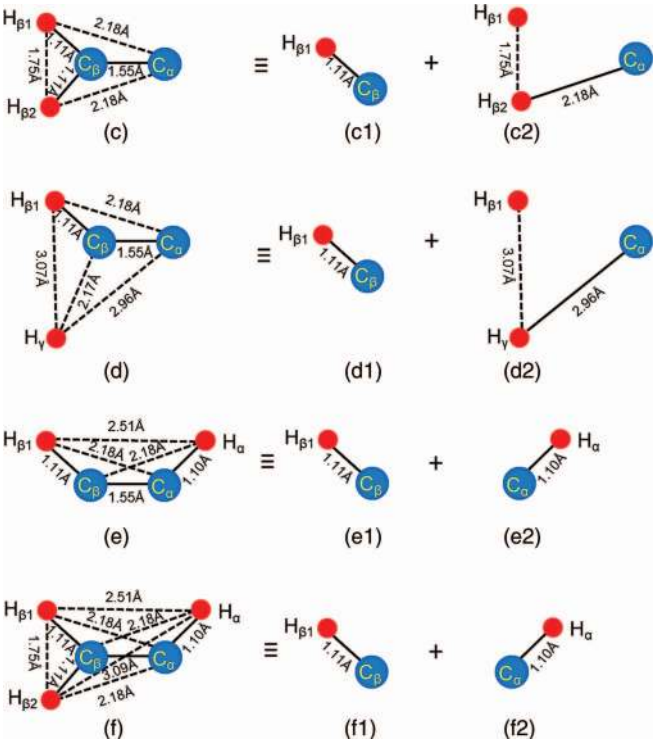

FIG. 7. Schematic decomposition of polarization transfer in the model systems depicted in Figure 1.

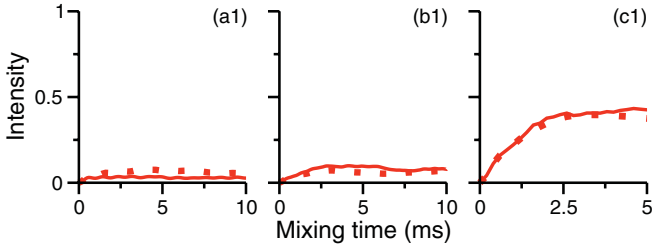

FIG. 8. Simulations depicting the polarization transfer to C_α in (a1) $C_\alpha H_{\beta 1} H_{\beta 2}$, (b1) $C_\alpha C_\beta H_{\beta 1} H_{\beta 2}$, and (c1) $C_\alpha H_\alpha C_\beta H_{\beta 1} H_{\beta 2}$ based on second-order recoupling (SOCP). The simulations were performed at $\upsilon_r = 60$ kHz and $\upsilon_{RF,C} = \upsilon_{RF,H} = 18$ kHz.

analytic simulations (based on effective Hamiltonians) depicting polarization transfer to C_α in SOCP experiments in model three ($C_\alpha H_{\beta 1} H_{\beta 2}$), four ($C_\alpha C_\beta H_{\beta 1} H_{\beta 2}$), and five-spin ($C_\alpha H_\alpha C_\beta H_{\beta 1} H_{\beta 2}$) systems are compared with exact numerical simulations (represented by dots).

Based on the effective Hamiltonian approach, polarization transfer in SOCP experiments is described through differential equations comprising of single-spin (e.g., $\Phi_0^{(1)}(\lambda, t)$, $\lambda = I_1, I_2, S$) and three-spin polarizations ($\Phi_0^{(k)}(I_i I_j S, t)$),

$$\begin{aligned} i\hbar \frac{d}{dt}\Phi_0^{(1)}(\lambda, t) &= \sum P^{(k)0}(I_i I_j S)\, \Phi_0^{(k)}(I_i I_j S, t), \\ i\hbar \frac{d}{dt}\Phi_0^{(k)}(I_i I_j S, t) &= \sum P^{(k_1)0}(I_i I_j S)\, \Phi_0^{(1)}(\lambda, t) \\ &\quad + \sum P^{(1)0}(\lambda)\, \Phi_0^{(k_1)}(I_i I_j S, t). \end{aligned} \tag{26}$$

Since polarization transfer in SOCP experiments is facilitated through three-spin operators, analytic descriptions based on the concept of effective Hamiltonians become less insightful when extended to larger groups of spin systems.

To explore the utility of truncated effective Hamiltonians in SOCP experiments, we begin our discussion with numerical simulations depicting polarization transfer to C_α in (a1) $C_\alpha H_{\beta 1} H_{\beta 2}$, (b1) $C_\alpha H_{\beta 1} H_\gamma$, and (c1) $C_\alpha H_\alpha H_{\beta 1}$ in Figure 9. The above three-spin models have been carefully chosen to illustrate the combined effects of homonuclear and heteronuclear dipolar couplings in the propagation of spin polarization in second-order CP experiments.

Since three-spin operators (resulting from (a) C_1–H_1 X C_1–H_2) (b) C_1–H_1 X H_1–H_2) facilitate the propagation of spin

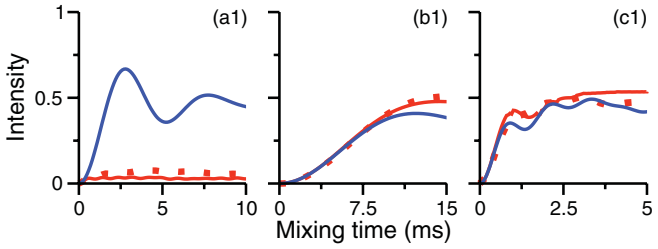

FIG. 9. Simulations depicting polarization transfer to C_α in model three-spin systems (a1) $C_\alpha H_{\beta 1} H_{\beta 2}$, (b1) $C_\alpha H_{\beta 1} H_\gamma$, and (c1) $C_\alpha H_\alpha H_{\beta 1}$ based on second-order recoupling (SOCP). The simulations were performed at $\upsilon_r = 60$ kHz and $\upsilon_{RF,C} = \upsilon_{RF,H} = 18$ kHz. The analytic simulations depicted in blue represent the absence of ^{1}H–^{1}H dipolar coupling in the reduced effective Hamiltonian.

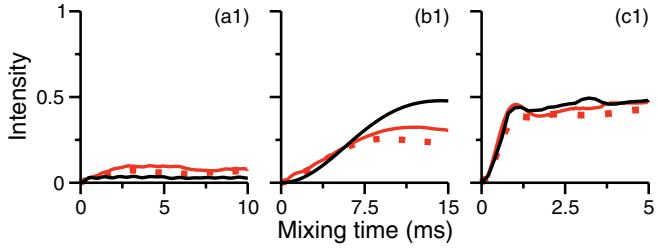

FIG. 10. Simulations depicting polarization transfer to C_α in model four-spin systems (a1) $C_\alpha C_\beta H_{\beta 1} H_{\beta 2}$, (b1) $C_\alpha C_\beta H_{\beta 1} H_\gamma$, and (c1) $C_\alpha H_\alpha C_\beta H_{\beta 1}$ based on second- order recoupling (SOCP). The simulations were performed at $\upsilon_r = 60$ kHz and $\upsilon_{RF,C} = \upsilon_{RF,H} = 18$ kHz. The analytic simulations depicted in black are derived from the three-spin model based on reduced effective Hamiltonian. The simulations depicted in red correspond to the four-spin model with solid lines depicting the analytic simulations (complete effective Hamiltonian) and dots denoting four-spin numerical simulations.

polarization in SOCP experiments, the simulations depicting the polarization transfer to C_α in $C_\alpha H_{\beta 1} H_{\beta 2}$ are bit counter-intuitive, given that the magnitude of the second-order three-spin coefficients (refer Table I) in $C_\alpha H_{\beta 1} H_{\beta 2}$ is greater in comparison to the three-spin models depicted in panels b1 and c1. To explain this anomalous result, we revisit the differential equations presented in Eq. (26).

In accord with the description of first-order based schemes, the coupled differential equations (see Eq. (26)) reduce to a much simpler form, when the magnitude of the coefficients associated with single-spin operators exceeds the magnitude of the three-spin coefficients (i.e., $P^{(1)0}(I_i) > P^{(k)0}(I_i I_j S)$),

$$\begin{aligned} i\hbar \frac{d}{dt}\Phi_0^{(1)}(\lambda, t) &= 0, \\ i\hbar \frac{d}{dt}\Phi_0^{(k)}(I_i I_j S, t) &= \sum P^{(1)0}(I_i)\, \Phi_0^{(k_1)}(I_i I_j S, t). \end{aligned} \tag{27}$$

Consequently, transfer of polarization among spins is inhibited in CP experiments. This aspect is exemplified in Figure 9 through a series of analytic simulations both in the presence (red) and absence of (depicted in blue) the second-order cross-terms resulting from the ^{1}H–^{1}H dipolar interactions. As illustrated (see panels 9b1, 9c1) in strongly coupled systems (a condition satisfied in systems comprising of directly bonded ^{13}C and ^{1}H), the second-order cross-terms due to ^{1}H–^{1}H dipolar interactions are of lesser consequence. Hence, in the weak-coupling limit, the stronger homonuclear coupling (^{1}H–^{1}H) truncates the heteronuclear coupling (^{13}C–^{1}H) and is primarily responsible for the depolarization observed in both first-order and second-order CP experiments. The above observations are in accord with our earlier description of polarization transfer from carbon to nitrogen in presence of protons.[26] Hence, the magnitude of the single-spin operators has a profound effect on the efficiency of polarization transfer in both first-order and second-order schemes.

To further substantiate the utility of the truncated effective Hamiltonians, polarization transfer to C_α in model four-spin systems (depicted in Figure 10) was investigated.

To minimize the complexity in the description, truncated effective Hamiltonians comprising of $T^{(k)0}(C_\beta H_{\beta 2} H_{\beta 1})$ and

single-spin operators (i.e., the stronger coupling due to $T^{(k)0}(C_\beta H_{\beta 2} H_{\beta 1})$ (resulting from cross-terms between $C_\beta H_{\beta 1} \times H_{\beta 1} H_{\beta 2}$) truncates $T^{(k)0}(C_\alpha H_{\beta 2} H_{\beta 1})$ (resulting from cross-terms between $C_\alpha H_{\beta 1} \times H_{\beta 1} H_{\beta 2}$) were employed to describe the polarization transfer observed in $C_\alpha C_\beta H_{\beta 1} H_{\beta 2}$. As depicted in Figure 10, the analytic simulations based on the truncated effective Hamiltonians (indicated in black) are in better agreement in $C_\alpha C_\beta H_{\beta 1} H_{\beta 2}$ (panel (a1)) and $C_\alpha H_\alpha C_\beta H_{\beta 1}$ (panel (c1)). The deviations observed in $C_\alpha C_\beta H_{\beta 1} H_\gamma$ (panel (b1)) may be due to stronger correlations among protons and are of lesser consequence in real systems. Hence, the polarization transfer to C_α in $C_\alpha H_\alpha C_\beta H_{\beta 1}$ is modeled by

$$H^{(eff)T}_{F,Four,C_\alpha} = \sum_{k=0}^{2} A^{(k)0}(C_\alpha H_{\beta_1} H_\alpha) T^{(k)0}(C_\alpha H_{\beta_1} H_\alpha) + \sum_{\lambda = C_\alpha, H_{\beta_1}, H_\alpha} B^{(1)0}(\lambda).iT^{(1)0}(\lambda). \quad (28)$$

In contrast to first-order based schemes, the ^{1}H–^{1}H dipolar interactions play an influential role in the propagation of spin polarization in second-order CP experiments. When the magnitude of the homonuclear coupling (among protons) exceeds the heteronuclear coupling, truncation (through second-order cross-terms) is observed both in first-order and second-order based schemes. On the contrary, as illustrated through models depicted in Figures 1(c) and 1(d), the dipolar truncation between heteronuclear spin pairs (^{13}C–^{1}H) facilitates the propagation of spin polarization in first-order based CP schemes. Hence, dipolar truncation remains the main driving force behind the propagation of polarization among spins in strongly coupled systems.

III. CONCLUSIONS

In summary, the current study elucidates the important role of dipolar truncation in the propagation of polarization from protons to carbons in CP experiments. Based on the phenomenon of truncation, an alternate framework in the form of truncated effective Hamiltonians is proposed to describe the propagation of spin polarization in strongly coupled systems. In contrast to the effective Hamiltonian approach, the present model facilitates the analytic description even in strongly coupled systems. Employing this approach, polarization transfer in first-order based CP experiments is described by a pseudo-three-spin model comprising of the active (^{13}C, ^{1}H) and passive spins. The effects of the ^{1}H–^{1}H dipolar interactions are incorporated through the longitudinal single-spin operators (protons) within the two-spin framework. In contrast to first-order based schemes, the ^{1}H–^{1}H-dipolar interactions play a dual role in the propagation of the spin polarization in second-order schemes. Hence, in a strongly coupled network, propagation of spin polarization across the sample is predominantly facilitated through the weakly coupled protons (^{1}H–^{1}H interaction) in the system. The current study presents a probable mechanism of propagation of spin polarization in CP experiments and could well be employed to build theoretical models for quantifying polarization transfer in strongly coupled spin systems.

ACKNOWLEDGMENTS

This research work was supported by a research grant to R.R. by the Department of Science and Technology (DST, SR/S1/PC-07/2008), Government of India and Z.Q. would like to thank IISERM for graduate assistantship.

APPENDIX: SUMMARY OF SECOND-ORDER CORRECTIONS

TABLE I. Second-order corrections to the effective Hamiltonian for a model three-spin system $I_1 I_2 S$. The spherical tensor operators have been constructed by sequential coupling[29] of the angular momentum vectors between the spins.[24] The constant "N" represents the number of spins and the results presented could be generalized for N-coupled (spin 1/2) systems. The indices p and q (can be integers/fractions) defined in the operators are due to $\omega_{RF,I} = p\omega_r$, $\omega_{RF,S} = q\omega_r$. In this article the following values of p and q have been employed: $p = \frac{2}{3}, q = \frac{1}{3}$ (in first-order schemes) and $p = q = 1$ (in second-order schemes).

Types of commutators	Coefficients	Operators
Single-spin operators		
(i) $\underbrace{\left[T^{(1)\pm 1}_{m\pm p}(I_1), T^{(1)\mp 1}_{-m\mp p}(I_1)\right]}_{\mathrm{CSA}\times\mathrm{CSA}}$	$\frac{G^{(1)\pm 1}_{m\pm p}(I_1).G^{(1)\mp 1}_{-m\mp p}(I_1)}{m\omega_r \pm \omega_{RF,I}}$	$\mp\left(\frac{1}{\sqrt{2}}\right)^{N-2} \frac{i}{2} T^{(1)0}_{\{1\}}(I_1)$
(ii) $\underbrace{\left[T^{(2)\pm 2}_{m\pm 2p}(I_1 I_2), T^{(2)\mp 2}_{-m\mp 2p}(I_1 I_2)\right]}_{\mathrm{DQ_{Homo}}\times\mathrm{DQ_{Homo}}}$	$\frac{G^{(2)\pm 2}_{m\pm 2p}(I_1 I_2).G^{(2)\mp 2}_{-m\mp 2p}(I_1 I_2)}{m\omega_r \pm 2\omega_{RF,I}}$	$\pm\left(\frac{1}{\sqrt{2}}\right)^{N-2} \frac{i}{2}\left[T^{(1)0}_{\{1\}}(I_1) + T^{(1)0}_{\{1\}}(I_2)\right]$
(iii) $\underbrace{\left[T^{(2)\pm 2}_{m\pm p\pm q}(I_1 S), T^{(2)\mp 2}_{-m\mp p\mp q)}(I_1 S)\right]}_{\mathrm{DQ_{Het}}\times\mathrm{DQ_{Het}}}$	$\frac{G^{(2)\pm 2}_{m\pm p\pm q}(I_1 S).G^{(2)\mp 2}_{-m\mp p\mp q)}(I_1 S)}{m\omega_r \pm \omega_{RF,I} \pm \omega_{RF,S}}$	$\pm\left(\frac{1}{\sqrt{2}}\right)^{N-2} \frac{i}{2}\left[T^{(1)0}_{\{0\}}(I_1) + T^{(1)0}_{\{0\}}(S)\right]$
Three-spin operators		
(i) $\underbrace{\left[T^{(2)\pm 2}_{m\pm 2p}(I_1 I_2), T^{(2)\mp 2}_{-m\mp p\mp q}(I_1 S)\right]}_{\mathrm{DQ_{Homo}}\times\mathrm{DQ_{Het}}}$	$\frac{G^{(2)\pm 2}_{m\pm 2p}(I_1 I_2).G^{(2)\mp 2}_{-m\mp p\mp q}(I_1 S)}{m\omega_r \pm 2\omega_{RF,I}}$	$\left(\frac{1}{\sqrt{2}}\right)^{N-3} \frac{i}{2}\begin{bmatrix} \pm\frac{1}{2\sqrt{5}} T^{(3)0}_{\{2\}}(I_1 I_2 S) + \frac{1}{2\sqrt{2}} T^{(2)0}_{\{2\}}(I_1 I_2 S) \pm \frac{1}{2}\sqrt{\frac{3}{10}} T^{(1)0}_{\{2\}}(I_1 I_2 S) \\ -\frac{1}{2\sqrt{6}} T^{(2)0}_{\{1\}}(I_1 I_2 S) \mp \frac{1}{2\sqrt{2}} T^{(1)0}_{\{1\}}(I_1 I_2 S) - \frac{1}{2\sqrt{3}} T^{(0)0}_{\{1\}}(I_1 I_2 S) \end{bmatrix}$

TABLE I. (*Continued.*)

Types of commutators	Coefficients	Operators
(ii) $\underbrace{\left[T^{(2)\pm2}_{m\pm2p}(I_1I_2),\, T^{(2)\mp2}_{-m\mp p\mp q}(I_2S)\right]}_{\mathrm{DQ_{Homo}\times DQ_{Het}}}$	$\frac{G^{(2)\pm2}_{m\pm2p}(I_1I_2).G^{(2)\mp2}_{-m\mp p\mp q}(I_2S)}{m\omega_r \pm 2\omega_{RF,I}}$	$\left(\frac{1}{\sqrt{2}}\right)^{N-3}\frac{i}{2}\left[\begin{array}{l}\pm\frac{1}{2\sqrt{5}}T^{(3)0}_{\{2\}}(I_1I_2S)+\frac{1}{2\sqrt{2}}T^{(2)0}_{\{2\}}(I_1I_2S)\pm\frac{1}{2}\sqrt{\frac{3}{10}}T^{(1)0}_{\{2\}}(I_1I_2S)\\ +\frac{1}{2\sqrt{6}}T^{(2)0}_{\{1\}}(I_1I_2S)\pm\frac{1}{2\sqrt{2}}T^{(1)0}_{\{1\}}(I_1I_2S)+\frac{1}{2\sqrt{3}}T^{(0)0}_{\{1\}}(I_1I_2S)\end{array}\right]$
(iii) $\underbrace{\left[T^{(2)\pm2}_{m\pm p\pm q}(I_1S),\, T^{(2)\mp2}_{-m\mp p\mp q}(I_2S)\right]}_{\mathrm{DQ_{Het}\times DQ_{Het}}}$	$\frac{G^{(2)\pm2}_{m\pm p\pm q}(I_1S).G^{(2)\mp2}_{-m\mp p\mp q)}(I_2S)}{m\omega_r \pm\omega_{RF,I}\pm\omega_{RF,S}}$	$\left(\frac{1}{\sqrt{2}}\right)^{N-3}\frac{i}{2}\left[\begin{array}{l}\pm\frac{1}{2\sqrt{5}}T^{(3)0}_{\{2\}}(I_1I_2S)\mp\frac{1}{\sqrt{30}}T^{(1)0}_{\{2\}}(I_1I_2S)+\frac{1}{\sqrt{6}}T^{(2)0}_{\{1\}}(I_1I_2S)\\ -\frac{1}{2\sqrt{3}}T^{(0)0}_{\{1\}}(I_1I_2S)\pm\frac{1}{\sqrt{6}}T^{(1)0}_{\{0\}}(I_1I_2S)\end{array}\right]$
(iv) $\underbrace{\left[T^{(2)0}_{m}(I_1I_2),\, T^{(2)0}_{-m\mp p\pm q}(I_1S)\right]}_{\mathrm{ZQ_{Homo}\times ZQ_{Het}}}$	$\frac{G^{(2)0}_{m}(I_1I_2).G^{(2)0}_{-m\mp p\pm q}(I_1S)}{m\omega_r}$	$\left(\frac{1}{\sqrt{2}}\right)^{N-3}\frac{i}{2}\left[-\frac{1}{2\sqrt{2}}T^{(2)0}_{\{2\}}(I_1I_2S)+\frac{1}{2\sqrt{6}}T^{(2)0}_{\{1\}}(I_1I_2S)-\frac{1}{2\sqrt{3}}T^{(0)0}_{\{1\}}(I_1I_2S)\right]$
$\underbrace{\left[T^{(2)0}_{m}(I_1I_2),\, T^{(2)0}_{-m\mp p\pm q}(I_2S)\right]}_{\mathrm{ZQ_{Homo}\times ZQ_{Het}}}$	$\frac{G^{(2)0}_{m}(I_1I_2).G^{(2)0}_{-m\mp p\pm q}(I_2S)}{m\omega_r}$	$\left(\frac{1}{\sqrt{2}}\right)^{N-3}\frac{i}{2}\left[-\frac{1}{2\sqrt{2}}T^{(2)0}_{\{2\}}(I_1I_2S)-\frac{1}{2\sqrt{6}}T^{(2)0}_{\{1\}}(I_1I_2S)+\frac{1}{2\sqrt{3}}T^{(0)0}_{\{1\}}(I_1I_2S)\right]$
(v) $\underbrace{\left[T^{(2)0}_{m}(I_1I_2),\, T^{(0)0}_{-m\mp p\pm q}(I_1S)\right]}_{\mathrm{ZQ_{Homo}\times ZQ_{Het}}}$	$\frac{G^{(2)0}_{m}(I_1I_2).G^{(0)0}_{-m\mp p\pm q}(I_1S)}{m\omega_r}$	$\left(\frac{1}{\sqrt{2}}\right)^{N-3}\frac{i}{2}\left[-\frac{1}{2}T^{(2)0}_{\{2\}}(I_1I_2S)-\frac{1}{2\sqrt{3}}T^{(2)0}_{\{1\}}(I_1I_2S)\right]$
$\underbrace{\left[T^{(2)0}_{m}(I_1I_2),\, T^{(0)0}_{-m\mp p\pm q}(I_2S)\right]}_{\mathrm{ZQ_{Homo}\times ZQ_{Het}}}$	$\frac{G^{(2)0}_{m}(I_1I_2).G^{(0)0}_{-m\mp p\pm q}(I_2S)}{m\omega_r}$	$\left(\frac{1}{\sqrt{2}}\right)^{N-3}\frac{i}{2}\left[-\frac{1}{2}T^{(2)0}_{\{2\}}(I_1I_2S)+\frac{1}{2\sqrt{3}}T^{(2)0}_{\{1\}}(I_1I_2S)\right]$
(vi) $\underbrace{\left[T^{(2)0}_{m\pm p\mp q}(I_1S),\, T^{(2)0}_{-m\mp p\pm q}(I_2S)\right]}_{\mathrm{ZQ_{Het}\times ZQ_{Het}}}$	$\frac{G^{(2)0}_{m\pm p\mp q}(I_1S).G^{(2)0}_{-m\mp p\pm q}(I_2S)}{m\omega_r}$	$\left(\frac{1}{\sqrt{2}}\right)^{N-3}\frac{i}{2}\left[-\frac{1}{\sqrt{6}}T^{(2)0}_{\{1\}}(I_1I_2S)-\frac{1}{2\sqrt{3}}T^{(0)0}_{\{1\}}(I_1I_2S)\right]$
(vii) $\underbrace{\left[T^{(2)0}_{m\pm p\mp q}(I_1S),\, T^{(0)0}_{-m\mp p\pm q}(I_2S)\right]}_{\mathrm{ZQ_{Het}\times ZQ_{Het}}}$	$\frac{G^{(2)0}_{m\pm p\mp q}(I_1S).G^{(0)0}_{-m\mp p\pm q}(I_2S)}{m\omega_r}$	$\left(\frac{1}{\sqrt{2}}\right)^{N-3}\frac{i}{2}\left[\frac{1}{2}T^{(2)0}_{\{2\}}(I_1I_2S)-\frac{1}{2\sqrt{3}}T^{(2)0}_{\{1\}}(I_1I_2S)\right]$
(viii) $\underbrace{\left[T^{(0)0}_{m\pm p\mp q}(I_1S),\, T^{(2)0}_{-m\mp p\pm q}(I_2S)\right]}_{\mathrm{ZQ_{Het}\times ZQ_{Het}}}$	$\frac{G^{(0)0}_{m\pm p\mp q}(I_1S).G^{(2)0}_{-m\mp p\pm q}(I_2S)}{m\omega_r}$	$\left(\frac{1}{\sqrt{2}}\right)^{N-3}\frac{i}{2}\left[-\frac{1}{2}T^{(2)0}_{\{2\}}(I_1I_2S)-\frac{1}{2\sqrt{3}}T^{(2)0}_{\{1\}}(I_1I_2S)\right]$
(ix) $\underbrace{\left[T^{(0)0}_{m\pm p\mp q}(I_1S),\, T^{(0)0}_{-m\mp p\pm q}(I_2S)\right]}_{\mathrm{ZQ_{Het}\times ZQ_{Het}}}$	$\frac{G^{(0)0}_{m\pm p\mp q}(I_1S).G^{(0)0}_{-m\mp p\pm q}(I_2S)}{m\omega_r}$	$\left(\frac{1}{\sqrt{2}}\right)^{N-3}\frac{i}{2}\left[\frac{1}{\sqrt{3}}T^{(0)0}_{\{1\}}(I_1I_2S)\right]$

[1] U. Haeberlen, *High-Resolution NMR in Solids: Selective Averaging* (Academic, New York, 1976).
[2] M. Mehring, *Principles of High Resolution NMR in Solids* (Springer-Verlag, Berlin, 1983).
[3] A. Abragam, *The Principles of Nuclear Magnetism* (Clarendon, Oxford, 1961).
[4] S. R. Hartmann and E. L. Hahn, Phys. Rev. **128**, 2042 (1962).
[5] E. R. Andrew, A. Bradbury, and R. G. Eades, Nature (London) **182**, 1659 (1958); I. J. Lowe, Phys. Rev. Lett. **2**, 285 (1959).
[6] A. Pines, M. G. Gibby, and J. S. Waugh, J. Chem. Phys. **59**, 569 (1973).
[7] E. O. Stejskal, J. Schaefer, and J. S. Waugh, J. Magn. Reson. **28**, 105 (1977); J. Schaefer and E. O. Stejskal, J. Am. Chem. Soc. **98**, 1031 (1976); J. Schaefer, E. O. Stejskal, J. R. Garbow, and R. A. McKay, J. Magn. Reson. **59**, 150 (1984).
[8] B. Q. Sun, P. R. Costa, and R. G. Griffin, J. Magn. Reson. A **112**, 191 (1995); X. Wu and K. W. Zilm, *ibid.* **104**, 154 (1993); S. Hediger, B. H. Meier, and R. R. Ernst, Chem. Phys. Lett. **213**, 627 (1993); J. Chem. Phys. **102**, 4000 (1995); Chem. Phys. Lett. **240**, 449 (1995); M. Baldus, D. G. Geurts, S. Hediger, and B. H. Meier, J. Magn. Reson. A **118**, 140 (1996); M. Baldus, A. T. Petkova, J. Herzfeld, and R. G. Griffin, Mol. Phys. **95**, 1197 (1998); M. Bjerring and N. C. Nielsen, Chem. Phys. Lett. **382**, 671 (2003); S. Laage, A. Marchetti, J. Sein, R. Pierattelli, H. J. Sass, S. Grzesiek, A. Lesage, G. Pintacuda, and L. Emsley, J. Am. Chem. Soc. **130**, 17216 (2008); G. Metz, X. Wu, and S. O. Smith, J. Magn. Reson. A **110**, 219 (1994).
[9] J.-P. Demers, V. Vijayan, S. Becker, and A. Lange, J. Magn. Reson. **205**, 216 (2010); G. D. Paepe, J. R. Lewandowski, A. Loquet, A. Bockmann, and R. G. Griffin, J. Chem. Phys. **129**, 245101 (2008); G. D. Paepe, J. R. Lewandowski, A. Loquet, M. Eddy, S. Megy, A. Bockmann, and R. G. Griffin, *ibid.* **134**, 095101 (2011).
[10] A. Lange, I. Scholz, T. Manolikas, M. Ernst, and B. H. Meier, Chem. Phys. Lett. **468**, 100 (2009).
[11] J. R. Lewandowski, G. D. Paepe, and R. G. Griffin, J. Am. Chem. Soc. **129**, 728 (2007).
[12] M. J. Bayro, M. Huber, R. Ramachandran, T. C. Davenport, B. H. Meier, M. Ernst, and R. G. Griffin, J. Chem. Phys. **130**, 114506 (2009).
[13] B. H. Meier, Chem. Phys. Lett. **188**, 201 (1992).
[14] C. P. Slichter, *Principles of Magnetic Resonance* (Springer, Heidelberg, 1990).
[15] V. Vijayan, J.-P. Demers, J. Biernat, E. Mandelkow, S. Becker, and A. Lange, Chem. Phys. Chem. **10**, 2205 (2009).
[16] M. Veshtort and R. G. Griffin, J. Magn. Reson. **178**, 248 (2006).
[17] M. M. Maricq and J. S. Waugh, J. Chem. Phys. **70**, 3300 (1979).
[18] U. Haeberlen and J. S. Waugh, Phys. Rev. **175**, 453 (1968).
[19] J. H. Shirley, Phys. Rev. B **4**, 979 (1965).
[20] R. Ramachandran and R. G. Griffin, J. Chem. Phys. **122**, 164502 (2005).
[21] R. Ramesh and M. S. Krishnan, J. Chem. Phys. **114**, 5967 (2001); E. Vinogradov, P. K. Madhu, and S. Vega, *ibid.* **115**(19), 8983 (2001); I. Scholz, J. D. v. Beek, and M. Ernst, Solid State Nucl. Magn. Reson. **37**, 39 (2010).
[22] R. Ramachandran and R. G. Griffin, J. Chem. Phys. **125**, 044510 (2006).
[23] R. Ramachandran, J. R. Lewandowski, P. C. A. V. D. Wel, and R. G. Griffin, J. Chem. Phys. **124**, 214107 (2006).
[24] R. Ramachandran, V. S. Bajaj, and R. G. Griffin, J. Chem. Phys. **122**, 164503 (2005).

[25]M. K. Pandey and M. S. Krishnan, J. Chem. Phys. **133**, 174121 (2010); M. K. Pandey and R. Ramachandran, Mol. Phys. **108**, 619 (2010).
[26]M. K. Pandey and R. Ramachandran, Mol. Phys. **109**, 1545 (2011).
[27]J. H. V. Vleck, Phys. Rev. **33**, 467 (1929); M. R. Aliev and V. T. Aleksanyan, Opt. Spectrosc. **24**, 520 (1968); **24**, 695 (1968); D. Papousek and M. R. Aliev, *Molecular Vibrational-Rotational Spectra* (Elsevier, Amsterdam, 1982).
[28]G. J. Boender, S. Vega, and H. J. M. d. Groot, Mol. Phys. **95**, 921 (1998).
[29]B. C. Sanctuary, J. Chem. Phys. **64**, 4352 (1976).
[30]B. C. Sanctuary and T. K. Halstead, Adv. Magn. Opt. Reson. **15**, 79 (1990).